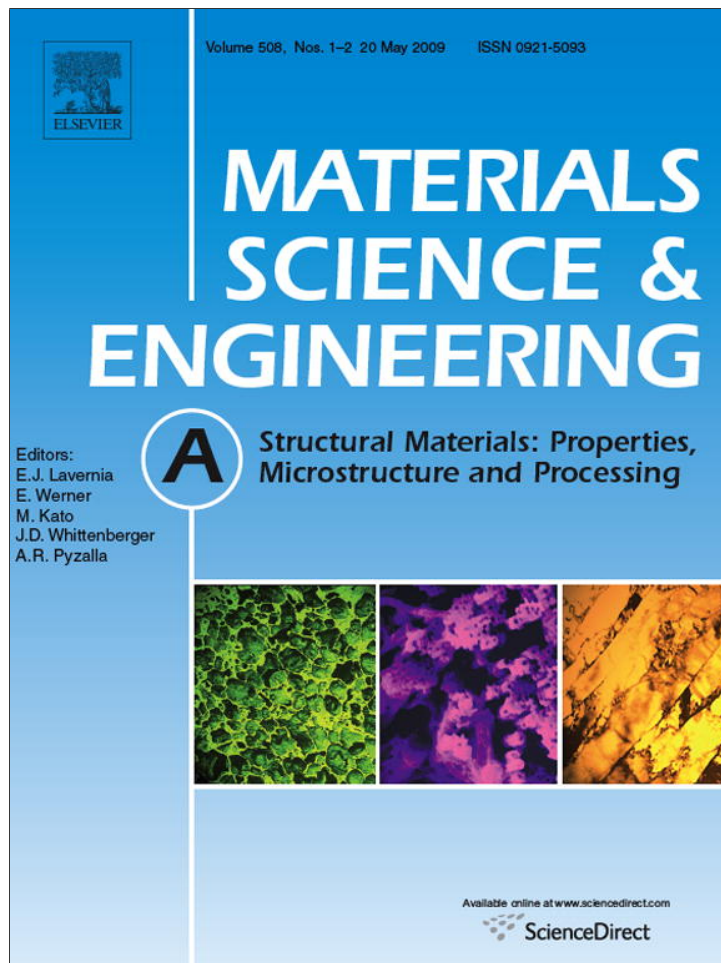


Provided for non-commercial research and education use.  
Not for reproduction, distribution or commercial use.



This article appeared in a journal published by Elsevier. The attached copy is furnished to the author for internal non-commercial research and education use, including for instruction at the authors institution and sharing with colleagues.

Other uses, including reproduction and distribution, or selling or licensing copies, or posting to personal, institutional or third party websites are prohibited.

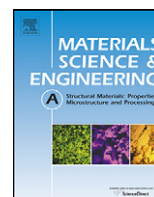
In most cases authors are permitted to post their version of the article (e.g. in Word or Tex form) to their personal website or institutional repository. Authors requiring further information regarding Elsevier's archiving and manuscript policies are encouraged to visit:

<http://www.elsevier.com/copyright>



Contents lists available at ScienceDirect

## Materials Science and Engineering A

journal homepage: [www.elsevier.com/locate/msea](http://www.elsevier.com/locate/msea)

# The effect of thickness on the creep response of thin-wall single crystal components

Brice Cassenti<sup>a</sup>, Alexander Staroselsky<sup>b,\*</sup>

<sup>a</sup> Rensselaer Polytechnic Institute, 275 Windsor St, Hartford, CT 06120, United States

<sup>b</sup> Pratt & Whitney, 400 Main Street, East Hartford, CT 06108, United States

## ARTICLE INFO

### Article history:

Received 26 March 2008

Received in revised form 16 December 2008

Accepted 22 December 2008

### Keywords:

Damage

Creep

Size effects

Dislocations

Surface roughness

## ABSTRACT

An understanding of the micromechanics of high temperature creep and damage accumulation in single crystal nickel base superalloys is important for the design of turbine blades and vanes in advanced commercial and military gas turbines. Advanced turbine blades are typically thin-walled cooled structures made of single crystal nickel base superalloys. Testing has shown that the creep response is larger in these thin wall structures than in test specimens typically used to characterize the material. It has also been experimentally observed that creep rupture lives obtained at moderate to high temperatures decreased sharply (~60%) with a reduction in specimen thickness by approximately eight times. We have developed a dislocation-based model to help explain this effect. The model considers the interaction of dislocations with the surface and the effect of nucleated intrusions or/and extrusions on creep strain rate.

© 2009 Elsevier B.V. All rights reserved.

## 1. Introduction

Advanced commercial and military engines are subjected to many rapid throttle movements and as a result, turbine airfoils experience a large number of thermo-mechanical fatigue (TMF) cycles. The severe loads experienced in long cruise missions have a long fraction of hot dwell time, which creates additional complications. Therefore, airfoil creep phenomena and especially creep–fatigue interaction become very important for reliable airfoil life prediction.

Both airfoil alloys and their protective coatings have advanced significantly in the last two decades. Ni-based superalloys have progressed from equiax microstructure to directionally solidified and finally to single crystal (SX) alloys with the improved creep and oxidation resistance. SX materials are highly anisotropic in both elastic and viscoplastic properties, which must be included in the design and life prediction process. Also, overall requirements for weight reduction and advanced metal cooling schemes drive designs toward thinning of the effective airfoil walls [1].

The effect of section thickness on creep deformation and the rupture properties of superalloy castings are extremely important in the design considerations and durability analysis of turbine airfoils [2]. Recent advances in airfoil design, particularly, state of the art microcircuit air cooling and refractory metal core (RMC) cooling schemes require significant reductions in the casting wall thickness

and, in turn, generate airfoil design with very thin walls. However, the successful design of advanced SX airfoils requires reliable local creep and rupture prediction associated with these scale effects.

The increase of creep strain rate and reduction of the creep rupture time under fixed nominal loading conditions with a decrease in the part thickness is called the thin wall debit. The thin wall debit observed for equiax grain casting was very significant when compared with the standard 0.25 in. bar creep tests [2]. Test results obtained in [2] on SX CMSX-3 showed that the thin section thickness debit in the stress rupture lives of uncoated specimens was considerable while the rupture lives of coated specimens were essentially independent of section thickness. Extensive testing of both coated and uncoated PWA 1480 specimens when the section thickness was reduced to 0.25 mm (10 mils) [3] demonstrated a debit of 30–40% in creep rupture strength for all conditions. These clearly illustrate that the thin wall debit depends on surface effects and specifically on degradation mechanisms taking place primarily in the specimen surface and subsurface zones.

Creep true strain vs. time relationships are shown in Fig. 1 for single crystal flat specimens of the Ni-based superalloy PWA 1484 at a nominally constant applied stress for variations in the specimen thickness by nearly an order of magnitude. The thinner the specimen is the earlier the tertiary creep regime starts and the shorter the time to rupture will be, as can be easily seen on graphs in Fig. 1.

A recent study of creep behavior of the single crystal nickel-base superalloy René N5 has also shown that reducing the thickness from 1.0 to 0.2 mm leads to both shorter creep lives and much higher overall creep strain rates of thin specimens [4].

\* Corresponding author. Tel.: +1 860 565 2751; fax: +1 860 755 5511.  
E-mail address: [Alexander.Staroselsky@pw.utc.com](mailto:Alexander.Staroselsky@pw.utc.com) (A. Staroselsky).

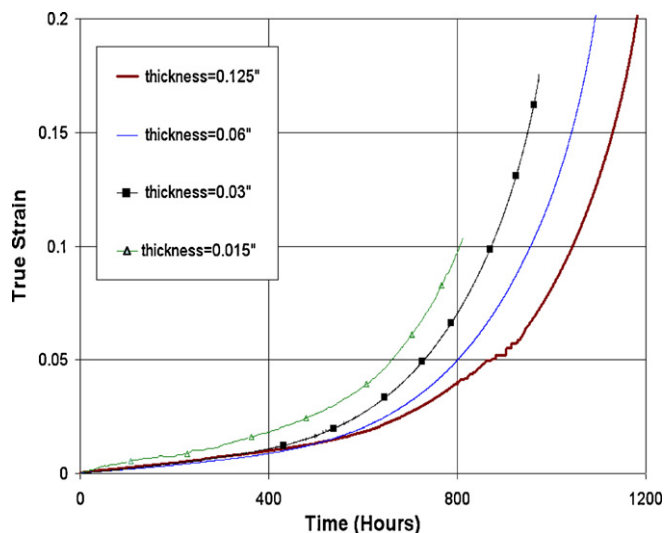


Fig. 1. Change of the rate of the creep deformation of a Ni-based superalloy single crystal with specimen thickness.

It is very important to emphasize the wide variety of different materials that demonstrate an increase of creep strain rate with a decrease of the specimen thickness. Ueno et al. [5] experimentally evaluated size effect on creep properties of lead free solders under several stress levels. They showed that the creep strain rate of thin specimens is higher than that of larger specimens. Another Japanese group Nitta and Itoh [6] observed the steady-state creep rate increase with decreasing specimen thickness (from 500 to 50  $\mu\text{m}$ ) of an Al–1%Si–0.5%Cu alloy, which is widely used for connections in microelectronic integrated circuits. Nes et al. [7] have also analyzed the increase in the creep rate of Al specimens. These authors considered the situation where the specimen diameter is comparable with the statistical dislocation slip length. All the above allows us to conclude that the “thin wall effect” is a generally observed phenomenon. In this paper we will focus our attention on Ni-based superalloys, however, the paper is of a methodological character and our results can be applied to other metals.

Systematic creep testing of flat SX specimens with different thicknesses can shed light on the thin section debit effect. Seetharaman and Cetel tested (001) oriented uncoated specimens of PWA 1484 in order to evaluate the thin section effect [8]. The specimens were machined from bulk single crystal castings eliminating the influence of such factors as variations in secondary dendrite arm spacing, micro-segregation patterns, micro-shrinkage, and porosity on the creep properties. In [8] the authors reported that time to 1% creep strain was found to be weakly dependent on the specimen thickness for all test conditions. However, they experimentally observed the biggest creep rupture life reduction due to the thickness debit was approximately 60%. This took place predominately at relatively low temperatures and high stresses. We might conclude from their results that (i) the effect does exist; and (ii) the effect manifests itself at moderate to large deformations. Therefore, the effect of a specimen thickness on creep is only noticeable when the dislocation structure is well developed and controls the damage accumulation and creep rate.

It is important to notice that two other specimen dimensions (the height = 0.75 in. and the width  $\sim$ 0.25 in.) are much larger than the specimen thickness in all tests, so, the observed effect cannot be explained by change of plain strain/plain stress conditions or amount of triaxiality.

Obviously, both experiments and practical experience demonstrate that the nature and extent of the thin wall debit are still not well understood and additional work needs to be done to explain,

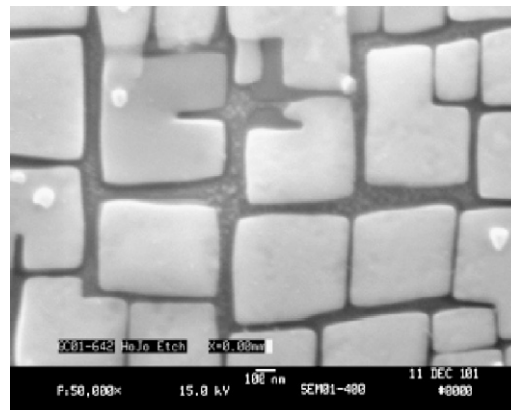


Fig. 2. Microstructures of fully heat treated PWA 1484 alloy [4].

and reliably predict, the amount of additional creep and damage associated with thin sections. Experimental data [2–4,8] known to the authors clearly demonstrate that the thin wall effect takes place if the section thickness becomes less than 20–40 mils (0.5–1 mm). Since the size of the  $\gamma'$  precipitates is less than 1  $\mu\text{m}$ , which is about three orders of magnitude smaller (see Fig. 2), the two-phase nature of intermetallic cannot be the direct cause of the observed effect. The typical size of the micro-pore is about 10–20  $\mu\text{m}$  [9] as shown in Fig. 3, which is also at least two orders of magnitude smaller than characteristic thickness. During the analyses we will assume that neither  $\gamma'$  particles nor initial porosity plays a significant role in the thin wall debit effect. Nevertheless, microstructure is crucial in modeling damage accumulation in order to predict creep curves.

Historically, secondary creep effects with associated modeling techniques (Larson–Miller, etc.) were used in engineering calculations. However, at high temperature Ni-based SX superalloys exhibit sigmoidal creep, where the creep rate drops fast to a minimum and then begins a continuous increase, effectively eliminating the secondary stage. Accurate creep models are essential for the development of successful designs in general and for the thin wall effect prediction in particular. In the model development the basic assumptions should be adequate to attack the problem but “do not complicate nature without necessity”. For creep modeling we assume a homogeneous single phased material with dislocation glide as a predominant deformation mode. However, we also need to consider damage accumulation (e.g., due to void growth) and the corresponding tertiary creep effects. The core of the presented constitutive model is at mesoscopic level, namely, dislocation dynamics, because the thin wall effect is associated with slip

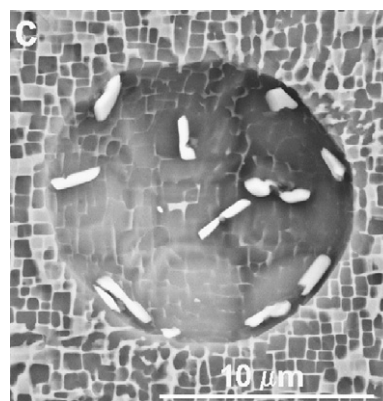


Fig. 3. Porosity in CMSX-10, cross-sections, SEM with round pore in undeformed material. Diameter is about 15  $\mu\text{m}$  [5].

line interactions with free surfaces. This makes the natural choice of the model scale at the dislocation loop level.

In a previous publication [10] we overviewed several damage mechanisms, namely multiplication of mobile dislocations; void and micro-crack growth and the scale effects caused by dislocation extrusions/intrusions and necking. Our damage model bridges the gap between dislocation dynamics and continuum mechanics scales. In this work we will concentrate on two major dislocation mechanisms causing the thin wall debit: (1) dislocation multiplication during creep deformation and (2) dislocation loop interactions with free surfaces resulting in extrusions/intrusions. Our model is based on a viscoplastic constitutive model which is discussed below.

It is worthwhile to note that the discussed effect of creep strength reduction with a decrease of the specimen thickness is completely opposite to the known scale effects in fracture mechanics [11] and plasticity [12]. In both these phenomena the strength of the specimen increases with a decrease in the specimen size. Despite different scale effects explanations based on the statistics of defect distributions in fracture mechanics, and on specific hardening due to strain gradients in plasticity, these mechanisms will predict a strength increase with a size decrease within reasonably broad limits. In this paper we consider the opposite effect specific for creep deformation. Hence, neither of these approaches can be employed for thin wall debit modeling. This is the first attempt to provide an explanation for such an effect.

The main objective of the presented work is to explain the thin wall debit in the creep rupture properties of a single crystal alloy. We have developed a dislocation-based viscoplastic model able to predict all stages of creep deformation: primary, secondary, and tertiary and deduced the statistical effect of dislocation loops interactions with free surfaces. Based on this analysis we formulated the model damage parameters and their evolution equations which allowed us to predict the thin wall debit effect in creep.

The plan of the paper is as follows: in the next section we formulate the constitutive viscoplastic model and couple it with dislocation kinetics. We will then introduce the thin wall model in Section 3. Creep model predictions will be compared against experimental data for a typical parameter set and we will close with some concluding remarks.

## 2. Viscoplastic model

It is generally accepted that creep deformation starts by the generation and glide of octahedral dislocations of the type  $\{111\}\langle 110 \rangle$  in  $\gamma$  channels. These dislocations overcome the  $\gamma'$  particle by a combination of slip and climb. It is also possible that the dislocations or their reaction products cut through the  $\gamma'$  particle if the applied stress is high enough to overcome the threshold. At high stresses and/or high temperatures the secondary cube slip systems  $\{100\}\langle 110 \rangle$  can also be activated. There are 12 octahedral slip systems and 6 cube slip systems in Ni-based superalloys. In bulk solids the inelastic flow is initiated by dislocations multiplication typically from Frank–Read sources. The dislocations glide, interacting with other dislocations in the solid and are immobilized, generating pinned dislocations. If the samples are thin, dislocation loops annihilate by interaction with the free surface creating intrusions or extrusions.

According to the Orowan assumption, creep strain rate is proportional to the density of the mobile dislocations  $\rho_m$ , magnitude of the Burgers vector,  $\mathbf{b}$ , and their average velocity. If we denote an arbitrary reference dislocation density throughout  $\rho_0$ , the dimensionless parameter  $\rho_m/\rho_0$  serves as a measure of the mobile dislocation density, and can be used to predict tertiary creep. We have used a standard viscoplastic power law creep with a back stress

[10] to represent the response of the material. The constitutive law for the inelastic strain,  $\gamma_i^p$  along slip plane  $i$  will be written as follows [13]:

$$\dot{\gamma}_i^p = \dot{\gamma}_0 \left( \frac{\rho_m}{\rho_0} \right) \left| \frac{\tau_i - \omega_i}{s_i^*} \right|^n \operatorname{sgn} \left( \frac{\tau_i - \omega_i}{s_i^*} \right) \exp \left( -\frac{Q}{kT} \right) \quad (1)$$

where  $\dot{\gamma}_0$  is a time constant,  $\tau_i$  is the slip plane resolved shear stress,  $s_i^*$  is the isotropic yield stress,  $\omega_i$  is the slip plane back stress, and  $(\dot{\cdot})$  is the rate of change with respect to time. The isotropic yield stress  $s_i^*$  is assumed to be a constant throughout this discussion but is actually a variable with its own evolution equation; exponential term represents the thermal activation process.

Primary creep is modeled by defining a slip system specific internal equilibrium stress variable  $\omega$ , which reflects redistribution of “internal resistance” with the strain. The back stress has a limiting saturation value corresponding to the end of primary creep stage and will be taken to evolve according to [14–16]:

$$\dot{\omega}_i = \lambda_0 |\dot{\gamma}_i^p| \left( \omega_\infty \sqrt{\frac{\rho_p}{\rho_p^{ss}}} \operatorname{sgn}(\dot{\gamma}_i^p) - \omega_i \right) \quad (2)$$

where  $\lambda_0$  is a time constant,  $\omega_\infty$  is the steady-state back stress,  $\rho_p$  is the pinned dislocation density, and  $\rho_p^{ss}$  is the value of the steady-state pinned dislocation density.

Back stress is used to characterize kinematic hardening and the effects of dynamic recovery [15]. The first term in (2) simulates the growth in the kinematic strain hardening with inelastic strain rate and the second term represents the rate of dynamic recovery. Dynamic equilibrium between hardening and recovery corresponds to the secondary creep stage and is simulated by the saturation value  $\omega_\infty$  of the state variable  $\omega$  in Eq. (2).

For completeness, the total strain, can be written as

$$\boldsymbol{\varepsilon} = \boldsymbol{\varepsilon}^e + \boldsymbol{\varepsilon}^p; \quad \boldsymbol{\varepsilon}^p = \frac{1}{2} \sum \gamma_i^p (\mathbf{m}^i \otimes \mathbf{n}^i + \mathbf{n}^i \otimes \mathbf{m}^i) \quad (3)$$

where  $\mathbf{m}$  and  $\mathbf{n}$  are the slip plane normal and slip direction correspondingly. This constitutive model is easily generalized to large deformation. In this work we use the twelve octahedral slip systems  $\langle 110 \rangle \langle 111 \rangle$ . At high temperatures the cube slip systems  $\langle 110 \rangle \langle 001 \rangle$  also contribute to the maintaining of the plastic flow of superalloys. However, the analyzed scale effect has been experimentally observed at moderate temperatures, so, without loss of generality, we can ignore the cube slip systems in this methodological study.

The initial conditions for these equations have the following form:

$$\omega_i = 0; \quad \gamma_i^p = 0 \quad @t = 0 \quad (4)$$

The mobile and the pinned dislocations densities will also evolve over time. Using concepts from chemical kinetics we have chosen to represent the evolution as two body interactions. We assume that dislocation immobilization takes place when two dislocation loops interact with each other. Our numerical experiments demonstrate that high order terms (e.g., three body interactions) do not bring any additional accuracy or noticeable changes in prediction. The density of mobile dislocations controls the strain rate, as one can see from Eq. (1), therefore, dislocation nucleation is the rate-limiting process. New dislocation pairs can be generated by Frank–Read sources in the bulk of solid.

Note from Eq. (1) that  $\dot{\gamma}_i^p$  is already a linear function of the mobile dislocation density and, hence, if the dislocation evolution equations vary linearly with the inelastic strain rate then to represent two body interactions they must also be proportional to a linear combination of the mobile and pinned dislocation densities. We assume that the dislocation density (for both mobile and pinned dislocations) increases with monotonic inelastic deformation and

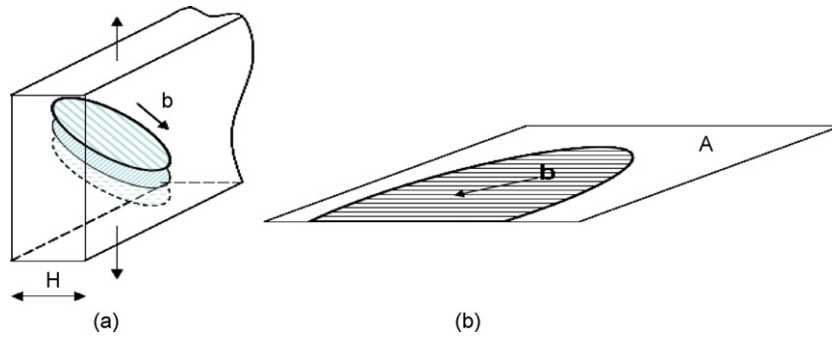


Fig. 4. Schematic representation of (a) dislocations loops in thin wall structures and (b) truncated by the free surface dislocation loop, leading to the surface “slip step”.

finally reaches a saturation value. Based on these assumptions, we have chosen the evolution equation for the mobile dislocation density to be [13]:

$$\frac{\dot{\rho}_m}{\rho_0} = \alpha \sum_{i=1}^{n_{slip}} \left( \frac{\tau_i - \omega_i}{s^*} \right) \dot{\gamma}_i^p \left( \frac{\varepsilon^2 \rho_m^{ss} + \rho_p^{ss} - \rho_p - \varepsilon^2 \rho_m}{\rho_0} \right) \quad (5)$$

where  $\alpha$  represents a time constant,  $\rho_m^{ss}$ , is the saturated mobile dislocation density,  $\rho_p^{ss}$ , is the saturated pinned dislocation density, and  $\varepsilon^2$  is a positive constant. Eq. (5) includes the annihilation of mobile dislocations and also includes their conversion to pinned dislocations. For the pinned dislocation density we have taken the evolution equation to be

$$\frac{\dot{\rho}_p}{\rho_0} = \beta \sum_{i=1}^{n_{slip}} \left( \frac{\tau_i - \omega_i}{s^*} \right) \dot{\gamma}_i^p \left( \frac{\rho_p^{ss} - \rho_p}{\rho_0} \right) \quad (6)$$

where  $\beta$  represents a time constant. The pinned dislocations grow at a rate that is proportional to the mobile dislocation density because of the presence of the plastic strain rate term. Throughout this paper, for the initial conditions we have taken

$$\rho_m = \rho_0; \quad \rho_p = 0 \quad @t = 0 \quad (7)$$

Of course, they can be generalized if the need arises.

This is stochastic process and the probability of source activation increases if the applied energy density approaches the barrier for dislocation nucleation [17]. Throughout this investigation we assume that the dislocation nucleation rate will increase with the inelastic slip shear strain,  $\gamma^i$ , and must always be positive. Dislocation generation and motion actually represents a non-recoverable state for the material. These states can be related to the energy of the system through equilibrium statistical mechanics. We postulate that dislocation generation rate is proportional to the entropy production,  $\dot{s}$ , which, in turn, is given by the following expression [10]:

$$\dot{s} = C \sum_{i=1}^{n_{slip}} \left( \frac{\tau_i - \omega_i}{s^*} \right) \dot{\gamma}_i^p \geq 0 \quad (8)$$

where the parameter  $C$  is a constant, and  $n_{slip}$  is the number of active slip systems. Note that in Eq. (8) the entropy production is always positive as can be seen by substituting for the strain rate using Eq. (1), and that the entropy production also appears naturally in Eqs. (5) and (6) used to describe the growth of the dislocation density. Hence the thermodynamics appears to be well represented.

### 3. Thin wall damage

We apply the mesoscale model outlined in the previous section to the explanation of the creep acceleration effect due to the reduced section thickness. The model parameters that might be

affected are resolved shear stress, elastic properties, and viscoplastic hardening. Here, we formulate the physical phenomena causing an increase in the applied effective stress and with any decrease of the cross-section and estimate the characteristics of the damaged surface layer.

We assume that: (1) dislocation loops are formed usually from Frank–Read type sources, and (2) the distance a dislocation loop moves is limited to the width of the sample. The loop will interact with the free surfaces as shown in Fig. 4 and result in truncated single arms of dislocations forming steps. Each step has a height at least equal to the lattice parameter.

The average total height of observed slip steps varies from several hundreds to several thousands of lattice parameters [18]. In thin samples, where the thicknesses are of the same order of magnitude as the radius of the dislocation loops, most of the loops end up forming the surface slip step as schematically shown in Fig. 4b. Accordingly, the model assumes a random distribution of dislocation loops with some of them ending at the surface. For a given dislocation, the length and the sign of the surface step (i.e., intrusion or extrusion) depends on Schmidt factors for the slip systems and can be considered as a random variable with a binomial distribution for the direction of the slip. In other words, first we consider slip band propagation and surface interceptions as a random walk process and then estimate the total height of surface slip steps. These steps will decrease the effective area over which shear stresses will act.

Recall that the thin-walled debit is based on the slip-induced surface roughness or in other words on the intersection of dislocation loops with the surface. Consider a flat dislocation loop of radius  $R$  with the normal to the plane of the loop at an angle  $\theta$  with respect to the direction of a uniaxial stress test specimen. It can be shown (details of the derivation can be found in Appendix A) that the average density of dislocation loops intercepting the surface,  $N_I$ , for a specimen of thickness  $H$  is

$$N_I = 4\rho_m \frac{\langle R \rangle}{H} \cos \theta \quad (9)$$

here  $\langle R \rangle$  is the average dislocation loop radius. Each surface step shifts the specimen surface in a direction (extrusion or intrusion, see Fig. 5) depending on the Burger’s vector orientation. For many dislocations intercepting the surface, the average number moving the surface right,  $\mu$  can be found from the binomial distribution as the half of total interceptions:

$$\mu = \frac{N_I}{2} \quad (10)$$

while the standard deviation,  $\sigma$ , satisfies

$$\sigma^2 = \frac{N_I W L}{4} \quad (11)$$

where  $W$  and  $L$  are the width and height (length) of a surface.

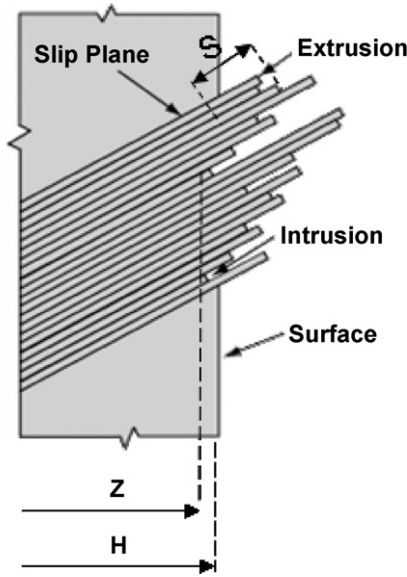


Fig. 5. Slip steps at the specimen surface causing reduction of effective cross-section; from [12].

Then for many interceptions, following the central limit theorem, we could assume the probability distribution in the number of intercepts is normal. If we substitute the mean value and standard deviation calculated in Eqs. (10) and (11) into a Gaussian distribution then we can obtain the average absolute distance,  $S$ , each surface moved from the mean:

$$S = \frac{b}{\sqrt{2\pi}} \sqrt{N_l WL} \quad (12)$$

where each dislocation has Burger's vector length  $b$ . Details of the derivation of Eq. (12) can be found in Appendix A.

It is important to emphasize that we describe here a mechanism of initiation of a damaged surface layer specific for the material structure. The proposed mechanism might be complimented by other surface effects such as, for example, oxidation or sub-surface microstructure degradation and we do not evaluate them in this methodological work. Our basic assumption is that this damaged surface layer is material structure specific and does not depend directly on loading scheme or geometry. Following surface damage initiation, the overstressed boundary layer is created, which in turn initiates the creation of active voids and micro-cracks and their subsequent growth.

We can find the increase in the cross-section stress by applying the fracture mechanics model for surface cracks of length  $S$  and average the local stress over the cross-section. Combining the applied stress,  $\sigma_0$ , with the averaged local effects we obtained the effective stress  $\sigma_L$  according to

$$\sigma_L = \frac{\sigma_0}{1 - 2S/H} \left( 1 + 2.24 \sqrt{\frac{S/H}{1 - 2S/H}} \right) \quad (13)$$

It can be seen that the effective stress depends on material parameter  $S$  and specimen thickness  $H$  and increases with the decrease of the specimen thickness. However, for relatively thick specimens, the effect of the damage layer is insignificant and does not cause a change in the creep strain rate prediction. Finally, note that the definition of how thick or thin the part section is related to the material specific surface damaged layer or on the scale parameter  $S/H$ . Of course the stress in Eq. (13) must also be used in the strain rates calculation.

Table 1  
Material parameters and initial conditions.

$\alpha$	4.00E+00	$\dot{\gamma}_0$	3.33E-10 s <sup>-1</sup>
$\beta$	4.00E+03	$\lambda$	1.00E+03
$G/s_0$	500	$\frac{\rho_p^{ss}}{\rho_0}$	4.00E+4
$n$	3	$\frac{\rho_m^{ss}}{\rho_0}$	4.00E+9
$\cos \theta$	0.5773	$\tau/s_0$	0.56
$\omega_\infty/s_0$	0.25	$\langle R \rangle/H$	3.33E-04
$H$	0.15 cm	WL	6.00 cm <sup>2</sup>
$b$	2.50E-08 cm		

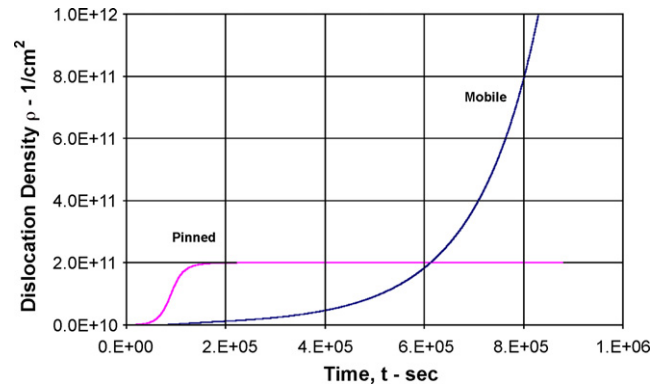


Fig. 6. Dislocation densities for data in Table 1.

#### 4. Numerical results and typical response

A typical creep response, that includes many of the effects that we represent, can be illustrated using the parameters and initial conditions shown in Table 1. The data in Table 1 has been taken to match the creep data in Ref. [8].

The dislocation density evolution is shown in Fig. 6. Initially the mobile dislocation density grows slowly. Later the pinned dislocation density levels out, and finally mobile dislocation density grows exponentially. These results also might give the explanation to the experimentally observed incubation period (about 2–4 h) in the primary creep curves of single crystal superalloys [19,20]. It is clear that the primary creep strain depends upon dislocation nucleation and propagation. One can see in Fig. 6 that some time is needed before the dislocation density reaches a level sufficient for maintaining a substantial creep flow. The fast saturation of pinned dislocations and the rise of the mobile dislocation density is specific for single crystal superalloys creep and results in the creep strain curve shown in Fig. 7.

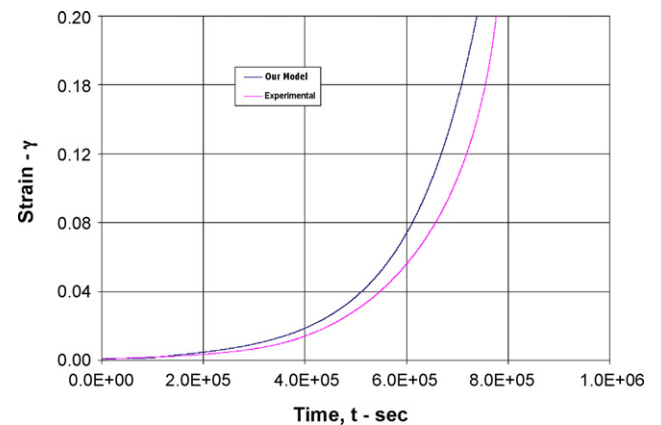


Fig. 7. Total strain for data in Table 1.

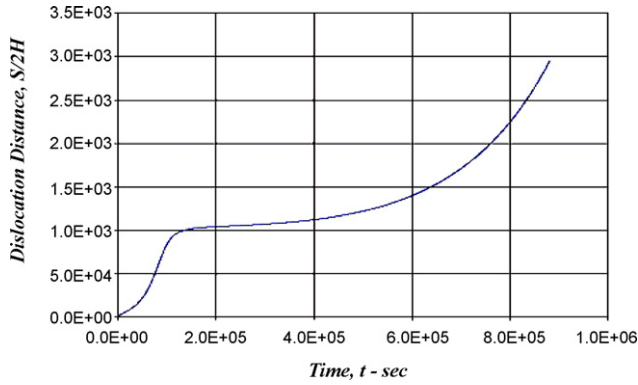


Fig. 8. Evolution of thin wall dislocation distance with time for data in Table 1.

Fig. 7 shows the total strain as a function of time. All three modes are actually present including a very short primary creep interval, a fairly long secondary creep region and a steep tertiary creep region.

The primary creep region is controlled by the rapidity with which the back stress and the pinned dislocations reach steady state. For Fig. 7 the primary creep region is short. The tertiary creep region is very steep (exponential raise) and is controlled by the growth of the mobile dislocation density. The developed model actually describes the observed “sigmoidal” creep where the tertiary part starts right after the primary stage. The steady part can be lengthened or shortened by changing the rates of the primary and tertiary creep response. Clearly, the initial conditions, such as the initial pinned and mobile dislocation density and the initial back stress would also control the length the primary, secondary and tertiary creep regions. We compare the model prediction against experimentally measured creep curve for PWA 1484 in (001) orientation under tension with the nominal stress of 248 MPa (36 ksi) at the temperature of 982 °C (1800 F). One can see that even for the rough parameters in Table 1, the agreement is satisfactory. For the low stress case considered (applied stress is 50% of the yield) the thin wall damage parameter is relatively small, but there is still a significant thin wall debit observed. The numerical results for the thin wall debit parameter ( $S/2H$ ) are shown in Fig. 8. Although  $S/2H$  is small, the change in the effective applied stress (see Eq. (13)) might reach 10% and ultimately the creep strain rate will become significant. Fig. 9 shows the creep time to reach a strain of 13% for different flat specimen thicknesses. The applied stress in this calculation has been chosen  $\tau/S_0 = 0.56$ . The calculated time decreases with a decrease in the specimen thickness  $H$ . Let us define the ratio

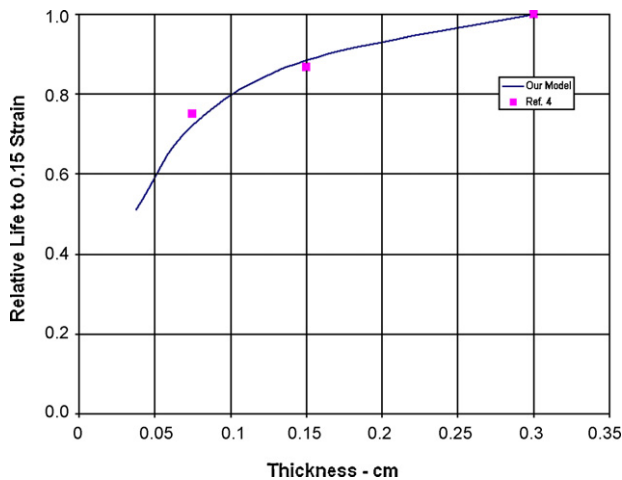


Fig. 9. Relative rupture life decrease example in thin wall structures.

of the calculated time to reach 13% strain to the corresponding time evaluated for the specimen of the thickness of 0.31 cm (125 mils) as the relative life. The relative life is shorter by 28% for 0.0375 cm (15 mils) and there is an evident decrease in the rupture life at a thickness below 0.15 cm (60 mils). The agreement with the test data in reference [8] is exceptional where the relative rupture life was found to decrease to 72% at a thickness of 0.075 cm (30 mils).

### 5. Conclusions

In this paper we analyzed the thickness debit effect reported during the creep tests of thin wall structures. A reduced section thickness leads to creep deformation greater than the observed creep response of thicker sections. The discussed effect is completely opposite to the known scale effects in fracture mechanics and plasticity where the structure strength increases with the decrease of the samples. Accounting for the debit in creep life is essential in the design of thin-wall single crystal structures deformation.

A dislocation-based material model has been presented for the creep analysis of single crystal superalloys. The model uses a multi-scale approach connecting interaction processes at the dislocation glide system level to the continuum creep behavior. Specific surface interaction mechanisms are thought to be required to predict a macroscopically observed scale dependent creep behavior. We show that an analysis of the statistical variation in the dislocation interception with the part free surface allows the introduction of scale parameter rationalizing much of the thin section creep debit effect. The performed creep calculations clearly demonstrate that the effects of the thickness debit can be explained by incorporation of the damage effects confined to the surface layer of the material. We can conclude that microscopic surface effects are important and have a significant effect on the macroscopic response of thin wall structures. These effects can be the motion of dislocations to the surface, the preferential generation of voids or micro-cracks near the surface, or even a direct result of surface oxidation. Our model of dislocation loops intersecting the surface shows that the important effect is the effective increase in stress if there are surface defects.

Comparison of the model predictions against known test results obtained on single crystals superalloys has shown good agreement with data. Experimental evidence [2] that thin wall debit effect of uncoated specimens was considerable while the rupture lives of coated specimens were essentially independent of section thickness strongly supports the model assumptions. However further microstructural analysis and experiments are necessary to fully quantify the effect of surface damage on thickness debit.

### Acknowledgement

Authors would like to thank Prof. Alan Needleman (Brown University) for numerous discussions and suggestions in the preparation of this document.

### Appendix A. Thin wall surface roughness

Consider a dislocation loop of radius  $R$  with its plane at an angle  $\theta$  with respect to the long axis of a tensile test specimen. Let the specimen have thickness  $H$  width  $W$  and length  $L$ . The projection of the loop on a surface perpendicular to the length is  $2R \cos \theta$ . If the dislocation loops have a uniform random distribution then the probability that the loop intersects one surface through the thickness  $H$  is  $2R/H \cos \theta$ . As long as  $R < H$  the probability to intersect

either surface,  $P_I$  is just

$$P_I = 2 \frac{R}{H} \cos \theta \quad (\text{A-1})$$

If we assume that many dislocations will intercept the surfaces, then the average number moving the surface to the right,  $\mu$  will be given by the binomial distribution as

$$\mu = \frac{N_I}{2} \quad (\text{A-2})$$

and the standard deviation,  $\sigma$ , will be for many interceptions, be

$$\sigma^2 = \frac{N_I W L}{4} \quad (\text{A-3})$$

Then for many interceptions, from the central limit theorem, the probability density,  $p_I$  for the distribution in the number of intercepts,  $x_I$ , is

$$P_I = \frac{1}{\sqrt{2\pi}\sigma} e^{-1/2(x_I/\sigma)^2} \quad (\text{A-4})$$

If each dislocation has Burger's vector length  $b$  then the largest deviation will be the average of the absolute value of  $b x_I$  (i.e.,  $\langle |b x_I| \rangle$ ). Let this average absolute distance be  $\bar{S}$ . Then

$$\begin{aligned} \bar{S} = \langle |b x_I| \rangle &= \int_{-\infty}^{\infty} \frac{b|x|}{\sqrt{2\pi}\sigma} e^{-1/2(x/\sigma)^2} dx = \frac{2b}{\sqrt{2\pi}\sigma} \int_0^{\infty} |x| e^{-1/2(x/\sigma)^2} dx \\ &= \frac{2\sigma b}{\sqrt{2\pi}} \quad (\text{A-5}) \end{aligned}$$

Substituting for  $\sigma$  in Eq. (A-5) using Eq. (A-3) the average absolute distance is

$$\bar{S} = \frac{b}{\sqrt{2\pi}} \sqrt{N_I W L} \quad (\text{A-6})$$

## References

- [1] B.L. Koff, J. Propul. Power 20 (2004) 577–595.
- [2] M. Doner, J.A. Heckler. Effects of Section Thickness and Orientation on Creep-Rupture properties of Two Advanced Single Crystal Alloys, in SAE Technical Paper #851785, Society of Automotive Eng.
- [3] F. Soechting, Thin Wall Debit, Internal Memo Pratt & Whitney, East Hartford, CT, 1982.
- [4] R. Hüttner, R. Völkl, J. Gabel, U. Glatzel, in: C. Reed, K.A. Green, P. Caron, T. Gabb, M. Fahrman, E. Huron, S. Woodard (Eds.), Creep Behavior of Thick and Thin Walled Structures of a Single Crystal Nickel-Base Superalloy at High Temperatures – Experimental Method and Results, Superalloys 2008, 2008, pp. 719–723.
- [5] A. Ueno, N. Takami, R. Sato, in: J. Pokluda (Ed.), Proceedings of the 17th European Conference of Fracture, Brno, Czech Republic, 2008, pp. 1120–1127.
- [6] T. Nitta, G. Itoh, Nippon Kinzoku Gakkaishi 63 (2) (1999) 196–200 (in Japanese).
- [7] E. Nes, W. Blum, P. Eisenlohr, Metal. Mater. Trans. A 33A (2002) 305–310.
- [8] V. Seetharaman, A. Cetel, in: K.A. Green, T.M. Pollock, H. Harada (Eds.), Thickness Debit in Creep Properties of PWA 1484, Superalloys 2004, 2004, pp. 207–213.
- [9] A. Epishin, T. Link, in: K.A. Green, T.M. Pollock, H. Harada (Eds.), Mechanisms of High Temperature Creep of Nickel-Base Superalloys Under Low Applied Stress, Superalloys 2004, 2004, pp. 137–143.
- [10] A. Staroselsky, B. Cassenti, in: E.E. Gdoutos (Ed.), Proceedings of the 16th European Conference of Fracture, Alexandroupolis, Greece, 2006.
- [11] A.M. Freudenthal, in: H. Liebowitz (Ed.), Fracture, vol. II, Academic Press, NY, 1968, pp. 591–621.
- [12] N.A. Fleck, J.W. Hutchinson, J. Mech. Phys. Solids 41 (1993) 1825–1857.
- [13] A. Staroselsky, B. Cassenti, Mech. Time-Depend. Mater. 12 (2008) 275–289.
- [14] D. Nissley, T. Meyer, K. Walker. Life Predictions and Constitutive Models for Engine Hot Section Anisotropic Materials, Pratt & Whitney, Report NAS3-23939, 1991.
- [15] D.C. Stouffer, L.T. Dame, Inelastic Deformation of Metals, John Wiley & Sons, Inc., NY, 1996, 502 p.
- [16] W. Xie, K.P. Walker, E.H. Jordan, M. Gell, J. Eng. Mater. Technol. 125 (2) (2003) 200–209.
- [17] A. Staroselsky, V. Bulatov, Multiscale Phenomena in Materials, vol. 578, MRS, 2000.
- [18] S. Kocanda, Fatigue Failure of Metals, Sijthoff & Noordhoff Int. Publishers, The Netherlands, 1978, 368 p.
- [19] D.W. Maclachlan, D.M. Knowles, Fatigue Fract. Eng. Mater. Struct. 25 (2002) 385–398.
- [20] F. Diologent, P. Caron, Mater. Sci. Eng. A 385 (1–2) (2004) 245–257.